

Extremal transmission through a microwave photonic crystal and the observation of edge states in a rectangular Dirac billiard

S. Bittner,¹ B. Dietz,^{1,*} M. Miski-Oglu,¹ and A. Richter^{1,2,†}

¹*Institut für Kernphysik, Technische Universität Darmstadt, D-64289 Darmstadt, Germany*

²*ECT*, Villa Tambosi, I-38123 Villazzano (Trento), Italy*

(Dated: April 9, 2022)

This article consists of two parts. First, we present transmission measurements of plane waves traversing a photonic crystal consisting of metallic cylinders which are arranged in a triangular lattice. The experiments are performed in the vicinity of a Dirac point, i.e., an isolated conical singularity of the photonic band structure. Exactly at the Dirac point the transmission shows a pseudodiffusive $1/L$ dependence, with L being the thickness of the crystal, a phenomenon also observed in graphene. Second, eigenmode intensity distributions measured in a microwave analog of a relativistic Dirac billiard, a rectangular microwave billiard that contains a photonic crystal, are discussed. Close to the Dirac point edge states have been detected, which are localized at the straight edge of the photonic crystal corresponding to a zigzag edge in graphene.

PACS numbers: 42.70.Qs, 73.22.Pr, 42.25.Fx

I. INTRODUCTION

The experimental realization of graphene¹, a one-atom-thick sheet of carbon atoms arranged in a honeycomb crystal lattice^{2,3}, attracted a lot of interest due to its peculiar electronic band structure which exhibits a linear dispersion at low energies. There the band structure closely resembles the spectrum of a relativistic massless spin one-half particle⁴. As a consequence, even though the Fermi velocity of electrons in graphene is only $c/300$ with c the speed of light, the electronic excitations are governed by the Dirac equation. The peculiar electronic properties lead to interesting physical phenomena^{4,5}.

The linear dispersion relation is entirely due to the threefold rotational symmetry of the hexagonal graphene lattice⁶. Therefore, graphene with its Dirac spectrum is not an exception. In general, systems comprising waves that propagate in a spatially periodic potential with the same symmetry properties can possess a Dirac spectrum. One example are so-called photonic crystals⁷, optical analogs of the common ones. It was shown theoretically in⁸ that under certain conditions photonic crystals with a triangular lattice geometry, shown schematically in Fig. 1, can exhibit the linear Dirac dispersion relation. The dependence of the frequencies f of propagating electromagnetic waves on the components (k_x, k_y) of the quasi-momentum vector exhibits a band structure which is similar to that for the electronic energies in graphene. The left hand side of Fig. 2 shows the first two bands obtained for a photonic crystal with cylinder radius $R = 0.25a$, where a is the lattice constant. It was calculated by numerically solving the Helmholtz equation using the finite difference method described in⁹. The two bands touch each other at the corners of the hexagonal Brillouin zone depicted in Fig. 2 where they have the shape of cones. Thus, there the frequencies of propagating modes depend linearly on the distance of the quasi-momentum from the touch points. The Brillouin zone

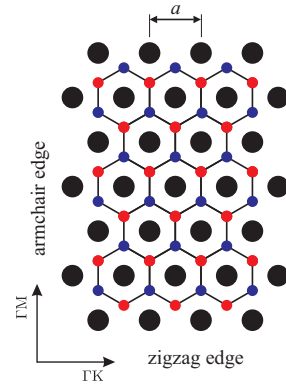


FIG. 1: (Color online) The triangular lattice of metallic cylinders. The voids between the cylinders are marked by colored circles. For graphene the red (bright) and the blue (dark) voids correspond to the two atoms which generate the two independent triangular sublattices. The arrows indicate the two directions ΓM and ΓK considered in the transmission experiments. The radius of the cylinders equals $R = 0.25a$, where a is the lattice constant.

comprises two non-equivalent corners \mathbf{K} and \mathbf{K}' that cannot be mapped onto each other by basis vectors of the reciprocal lattice. The band diagram closely resembles that of the electronic energies in graphene¹⁰. Accordingly, as in graphene¹¹ the touch points are referred to as Dirac points.

The photonic crystals also exhibits a hexagonal configuration. In fact, three neighboring cylinders forming a triangular cell of the photonic crystal lattice shown in Fig. 1 host quasibound states¹² localized at their center. The cell thus can be considered as an open resonator and the triangular lattice can be regarded as being built of coupled resonators, the voids between the cylinders acting as the atoms forming the two independent triangular sublattices that generate the honeycomb structure. In Fig. 1 the voids corresponding to the two sublattices are

marked with blue and red circles, respectively. The void structure terminates with a zigzag edge in the ΓK and with an armchair edge in the ΓM direction, respectively. These are the two most common types of boundaries arising from the hexagonal structure of graphene.

In the vicinity of the Dirac points the Schrödinger equation for the electrons in graphene^{4,13,14} and the Helmholtz equation governing the electromagnetic wave propagation in the photonic crystal⁸ reduce to two copies of the Dirac equation for massless relativistic spin one-half particles, one copy holding around \mathbf{K} and the other around \mathbf{K}' . Thus, photonic crystals can be used to investigate properties of graphene, as was done in analog experiments with microwave photonic crystals^{15–17} and also with sonic crystals¹⁸. There phenomena directly related to the linear dispersion relation around a Dirac point were investigated. We consider here two of them, the extremal transmission and the formation of edge states^{13,19,20}.

The Dirac dispersion relation affects the transport properties of photonic crystals in a remarkable way. It was shown theoretically in¹⁹ that at the Dirac point the intensity of electromagnetic waves transmitted through a photonic crystal is inversely proportional to the thickness of the crystal. This is different from the ballistic behavior and the exponential decay observed, respectively, in a band region and a gap region, but rather reminiscent of the diffusion behavior of waves traveling through a disordered medium. A similar behavior was predicted for the conductivity of an ideal graphene strip^{20,21}. We present below results on the experimental investigation of the transmission of electromagnetic waves traversing a microwave photonic crystal. The measurements (see Sec. II A) were performed close to a Dirac point, which was located as described in¹⁷.

In further experiments (see Sec. II B) we have inves-

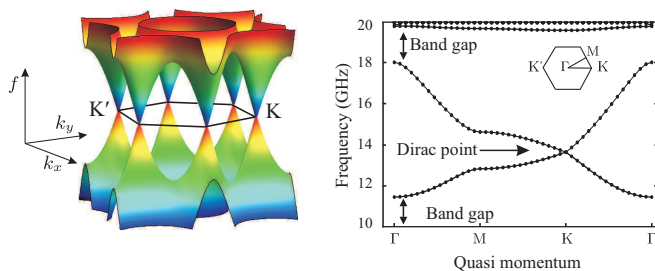


FIG. 2: (Color online) Left: numerically calculated band structure $f(k_x, k_y)$ as function of the quasi-momentum components (k_x, k_y) . Shown are the first and the second band. Blue (darkest) color corresponds to the lowest, red (brightest) color to the largest values of f within a band. The hexagonal Brillouin zone with the two non-equivalent K points \mathbf{K} and \mathbf{K}' is indicated. Right: band structure computed numerically by varying the quasi-momentum vector along the path $\Gamma MK\Gamma$ defining the boundary of the irreducible Brillouin zone depicted together with the Brillouin zone in the inset. Adopted from¹⁷.

tigated edge effects^{4,22,23} on the spectral properties^{24,25} of a microwave Dirac billiard, a microwave-analogue of graphene flakes. It is known that the spectrum of a graphene flake depends on the geometry of its edges^{24–26}. It has been shown that for a graphene flake terminated with armchair edges the density of states vanishes at the Dirac point such that a gap opens up in the band structure, whereas zigzag edges yield a nonvanishing density. Indeed, graphene flakes which terminate with zigzag edges or with both armchair and zigzag edges exhibit edge states in the vicinity of the Dirac point, which are localized close to the zigzag parts of its boundary. This property is attributed to the boundary conditions^{23,27} which differ for both types of edges. To verify the existence of such states the photonic crystal was enclosed in a metallic box.

II. EXPERIMENTS WITH THE MICROWAVE PHOTONIC CRYSTAL

Analog experiments with flat, cylindrical microwave cavities have been performed to model generic properties of quantum chaotic systems and of chaotic quantum scattering systems^{28–34}. This is possible in a range $f \leq f_{\max}$ of the excitation frequency f , where the wave length is longer than twice the height of the cavity. There, the electric field vector \vec{E} is perpendicular to the bottom and the top plates of the cavity and the vectorial Helmholtz equation reduces to a scalar one which is mathematically equivalent to the two-dimensional stationary Schrödinger equation for a quantum billiard of corresponding shape^{28–30}. Due to this analogy flat microwave cavities are commonly called microwave billiards. We used microwave photonic crystals consisting of metallic cylinders arranged in a triangular lattice (see Fig. 1) to model single particle properties of graphene. The experiments are described in Sec. II A and Sec. II B, respectively.

A. Extremal transmission at the Dirac frequency

For the experimental investigation of the transmission properties of a photonic crystal with a Dirac spectrum we used the setup shown in Fig. 3. The photonic crystal consisted of 960 cylinders with radius $R = 5$ mm and height $h = 8$ mm. To ensure a good electrical contact and thus reproducibility of the measurement each cylinder was screwed to the top and the bottom plate. The resulting photonic crystal contained 40 rows of 24 cylinders and had side lengths of, respectively, 400 mm and 859 mm. The height of the cylinders defined the maximal frequency $f_{\max} = 18.75$ GHz up to which the system was two dimensional. A two dimensional horn antenna emitted approximately plane waves and a waveguide antenna received waves transmitted through the crystal. Both antennas were tightly screwed to the top plate and

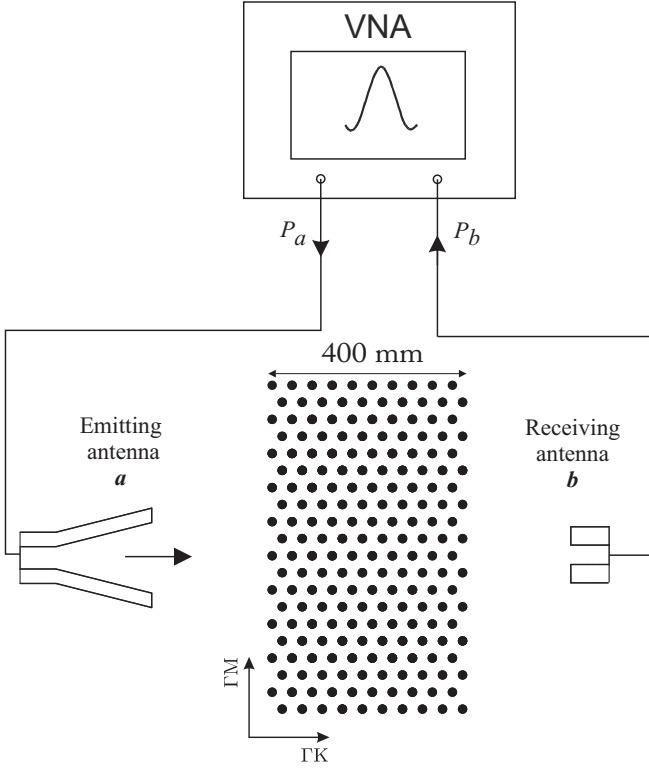


FIG. 3: Experimental setup (not to scale). The photonic crystal consisted of 960 copper cylinders arranged in a triangular lattice. Approximately plane waves were emitted by the microwave horn antenna and the transmitted signal was received by a waveguide antenna. The plane waves impinged the crystal in ΓK direction, in distinction to the experiments described in¹⁷ where the plane waves were sent onto the crystal in ΓM direction.

attached to waveguide-to-coaxial adapters. The transmission spectra were obtained with an Agilent PNA-L N5230A vectorial network analyzer (VNA). It measures the ratio of the power P_b of the signal received at the waveguide antenna and the power P_a of that emitted from the horn antenna and their relative phase. The modulus square of the transmission matrix element S_{ba} is given as

$$|S_{ba}(f)|^2 = \frac{P_b}{P_a}. \quad (1)$$

While in the experiments described in¹⁷ the plane waves impinged the crystal in ΓM direction, the transmission spectra shown in Fig. 4 were measured in ΓK direction (see Fig. 2) for different configurations of the experimental setup. First, the transmission spectrum was measured for the setup with 40 rows and then, step by step one row was removed from each armchair edge of the crystal. The three panels show exemplarily the spectra measured for crystals consisting of 8, 18, and 36 rows of cylinders, respectively. In all spectra the transmission is suppressed below 11.8 GHz. There, the band structure exhibits a gap (see right panel of Fig. 2). Below that frequency electro-

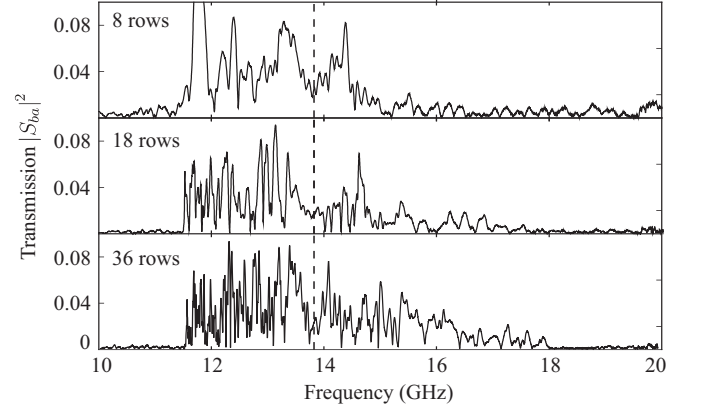


FIG. 4: Examples of transmission spectra measured with the setup shown in Fig. 3 in ΓK direction through a lattice with, respectively, 8, 18, and 36 rows of cylinders. The dashed line marks the Dirac frequency.

magnetic waves cannot propagate in the photonic crystal. Furthermore, the transmission spectra show a characteristic dip around the Dirac frequency $f_D = 13.8$ GHz, which was determined experimentally in¹⁷ and is marked in Fig. 4 with a dashed line.

To reveal the $1/L$ scaling, with L denoting the crystal thickness, of the transmitted power $|S_{ba}(f)|^2$ predicted at the Dirac point, we show in Fig. 5 the quantity $L|S_{ba}(f)|^2$ versus L for three different frequencies. In all three panels the filled circles are the experimental data. They are joined by dashed lines to guide the eye. The smooth curves depict the average behavior as function of L . The oscillations around the mean are attributed to standing waves arising between the antennas and the interfaces of the photonic crystal. The top panel shows the behavior of $L|S_{ba}|^2$ for $f = 13.18$ GHz, where the transmission is nonvanishing. In this frequency regime $L|S_{ba}|^2$ grows linearly with L , that is, the transmission $|S_{ba}|^2$ itself does not depend on L , as expected in band regions. The bottom panel of Fig. 5 shows the variation of $L|S_{ba}|^2$ with L for $f = 18.7$ GHz. This frequency lies within a stop band. As expected the transmission decreases exponentially with the crystal thickness L . The middle panel shows $L|S_{ba}|^2$ versus L at the Dirac frequency $f_D = 13.8$ GHz. There, the average behavior of $L|S_{ba}|^2$ is constant over a wide range of the crystal thickness. Thus, as shown in¹⁹, the transmission of plane waves, traveling in ΓK direction and excited with the Dirac frequency, through the photonic crystal scales with $1/L$. This is similar to the diffusion behavior of waves through a random medium. As was pointed out in³⁵ this phenomenon of extremal transmission is due to the linear Dirac dispersion relation. Note that its observation crucially depends on the orientation of the photonic crystal with respect to the incident plane waves. When emitting plane waves excited with the Dirac frequency in ΓM direction, as was done in previous experiments^{17,18}, the band structure has a partial band gap (see right panel of

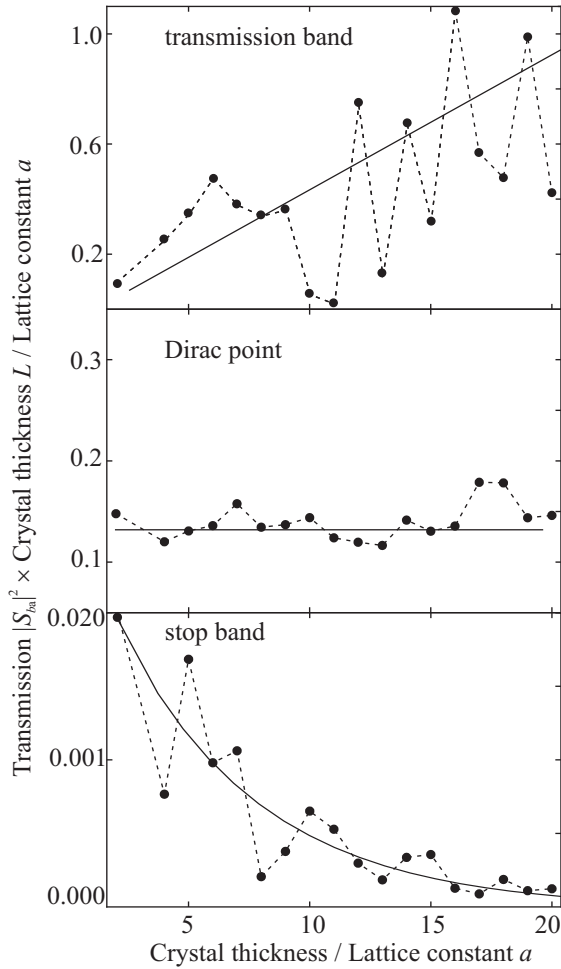


FIG. 5: The product of the transmission $|S_{ba}(f)|^2$ through the photonic crystal and its thickness L in units of the lattice constant a as function of L for different frequencies, from top to bottom for 13.18 GHz, 13.8 GHz, and 18.7 GHz. The filled circles are experimental data. They are joined with dashed lines to guide the eye. The solid lines result from the fits of a linear, a constant and an exponential function, respectively, to the data points.

Fig. 2). Accordingly, the transmission $|S_{ba}|^2$ decreases exponentially with the crystal thickness L . Thus, the decay length of the evanescent waves is finite, whereas it is infinite when exciting the Dirac point, e.g., by sending plane waves at the Dirac frequency in ΓK direction onto the crystal (see right panel of Fig. 2). The $1/L$ scaling at the Dirac point has been derived for photonic crystals in¹⁹. For this the solutions of the Helmholtz equation in free space were matched at the interface of the crystal to those of the Dirac equation, which is applicable inside the photonic crystal. Furthermore, conservation of the component of the wave vector parallel to the interface, that is, Snell's law, and of the flux through the boundary had to be taken into account. This yielded for the total

transmission T

$$T \propto \frac{W}{L}, \quad (2)$$

where W is the width of the photonic crystal, that is, in our case its extension in ΓM direction (see Fig. 3). The experimental results confirm the validity of Eq. (2) at the Dirac point.

Similar experiments were performed with photonic crystal consisting of dielectric rods with a high permittivity. Electromagnetic waves can stay longer in such a photonic crystal¹⁵. As a consequence, oscillations of the total transmission were observed for a crystal orientation with respect to the incident plane waves as in our experiment which are due to the scattering between the valleys \mathbf{K} and \mathbf{K}' . This is not possible in the present experiments with metallic cylinders. Instead, the oscillations observed in Fig. 5 are due to the formation of standing waves between the antennas and the crystal interfaces.

B. Edge states in a rectangular Dirac billiard

A motivation for the experiments presented in this section has been Ref.³⁶ where Berry and Mondragon considered the Dirac equation for massless spin one-half particles confined to a two-dimensional domain by introducing an infinite-mass term along its boundary, i.e., so-called neutrino billiards. Since close to the Dirac frequency the propagation of electromagnetic waves in a photonic crystal can be effectively described by the Dirac equation, below $f = f_{\max}$ a microwave photonic crystal enclosed in a metallic box provides an experimental setup for the investigation of spectral properties of relativistic quantum particles put inside a potential well. The reflection of electromagnetic waves at the walls of the metallic box, where the electric field strength obeys Dirichlet boundary conditions, leads to an excitation of states in both the valleys at \mathbf{K} and \mathbf{K}' of the associated band structure. Their coupling depends on the edge structure. Therefore, in distinction to neutrino billiards, such systems are governed by two Dirac equations, which are coupled depending on the shape of the metallic box enclosing the crystal^{13,25}. They are generally called Dirac billiards^{24,26}. Figure 6 shows a photograph of the experimental realization of a rectangular Dirac billiard. The photonic crystal has the same lattice constant a and the cylinders have the same radius R as in the scattering experiment described in Sec. II A. It is surrounded by a brass frame (the top plate has been removed for the photograph). In the experiments all cylinders and the frame were squeezed between the top and bottom plates with screws to ensure an optimal electrical contact. To measure transmission spectra wire antennas of 1 mm diameter were lowered into the resonator through 3 mm wide drillings in the top plate. The positions of the antennas are marked by white crosses in Fig. 6.

The top panel of Fig. 7 shows a measured transmission spectrum of the Dirac billiard. The positions of the

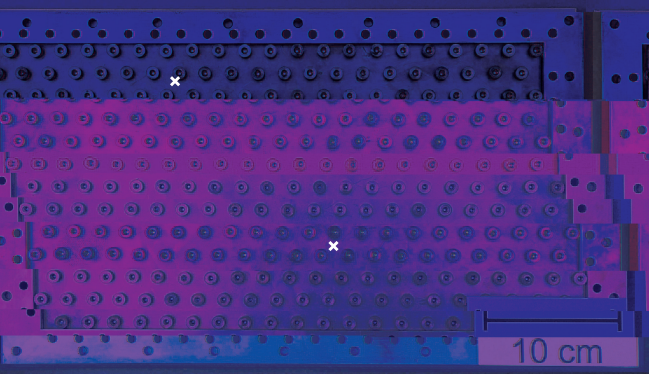


FIG. 6: (Color online) Photograph of the Dirac billiard with the top plate removed. The photonic crystal with triangular lattice is enclosed by a rectangular brass frame. The two white crosses mark the positions of the antennas.

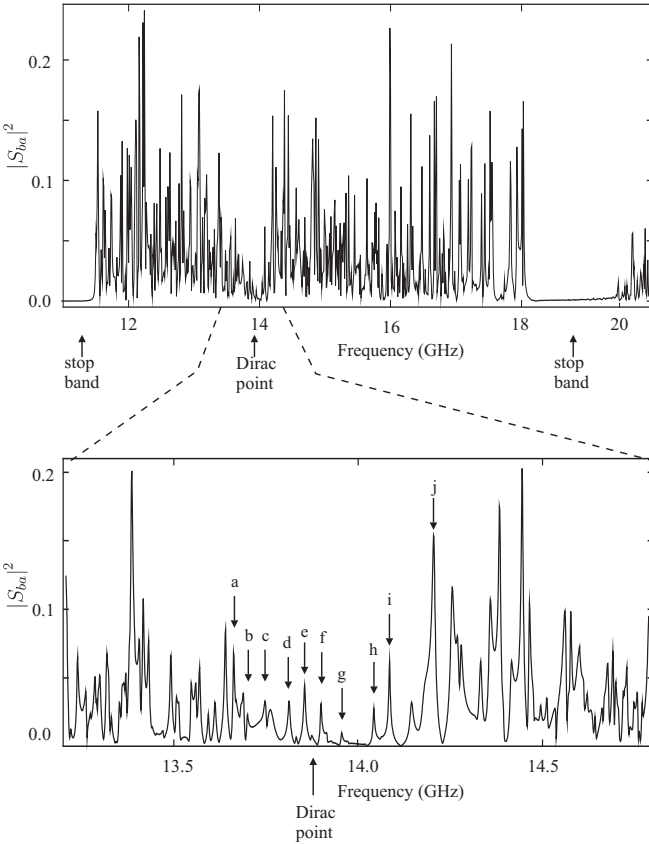


FIG. 7: Top panel: transmission spectrum measured between two wire antennas. Bottom panel: magnification of the spectrum in a region around the Dirac point. The arrows mark the resonance frequencies for which the measured electrical field intensity distributions are shown on Fig. 8. The labels of the resonances refer to the panels in Fig. 8.

resonance maxima yield the eigenvalues of the Dirac billiard. The stop band between 18 and 20 GHz is well pronounced. As in the scattering experiment described in Sect. II A we observe a dip around the Dirac frequency

$f_D = 13.8$ GHz, which is marked with an arrow. The bottom panel of Fig. 7 shows a magnified section of the transmission spectrum around the Dirac point. The spectrum contains sharp resonances and many overlapping ones. The latter render the extraction of the complete sequence of resonance frequencies impossible. However, a complete sequence of the eigenvalues of the corresponding Dirac billiard is needed for the study of its spectral fluctuation properties. This corroborates the necessity of the measurement of the spectra at superconducting conditions^{37,38}. Still, the experimental setup can be used to investigate properties of the associated wave functions, such as the appearance of edge states.

The wave functions of a quantum billiard are directly related to the electric field strength distributions in the corresponding microwave billiard at the resonance frequencies³⁰. Thus, their intensities can be determined experimentally by measuring the electric field intensity distributions. This was done with the help of the so-called perturbation body method^{28,39,40}, which is based on the Maier-Slater theorem⁴¹. A small perturbation body is inserted into the cavity. This induces a shift of the resonance frequencies the size of which depends on the electric and magnetic field strengths at the position of the perturbation body. Since we are only interested in the intensity distribution of the wave functions of the corresponding Dirac billiard, we used a perturbation body made from magnetic rubber⁴². In order to obtain the spatial distribution of the electric field strength the perturbation body was moved inside the closed microwave resonator with an external guiding magnet which is placed on a computer controlled positioning unit. The measurements were performed between the 14 rows of cylinders which are parallel to the long edges of the billiard. Each scan of the field intensity distribution was obtained by moving the perturbation body in 2 mm steps.

Figure 8 shows exemplarily ten electric field intensity distributions measured at resonance frequencies around the Dirac frequency. The labels of the panels correspond to the associated resonances in Fig. 7. The intensity patterns shown in Figs. 8 a and j are extended over the whole area of the microwave billiard. The structure of these intensity distributions resembles that of modes of the corresponding empty rectangular quantum billiard with one excitation parallel to the short billiard edge and several parallel to the long one. On the contrary, the intensity distributions shown in panels Fig. 8 e - h are localized close to the long edge of the rectangular billiard. In panels b - d we again observe the highest intensities close to long edge, but also nonvanishing intensities in the interior. At the long edge the photonic crystal terminates with a straight edge corresponding to a zigzag edge in graphene (see Fig. 1). States which are localized close to the armchair edge were not observed¹⁶. These experimental results confirm the prediction of defect states localized at the zigzag parts of the boundary of graphene flakes.

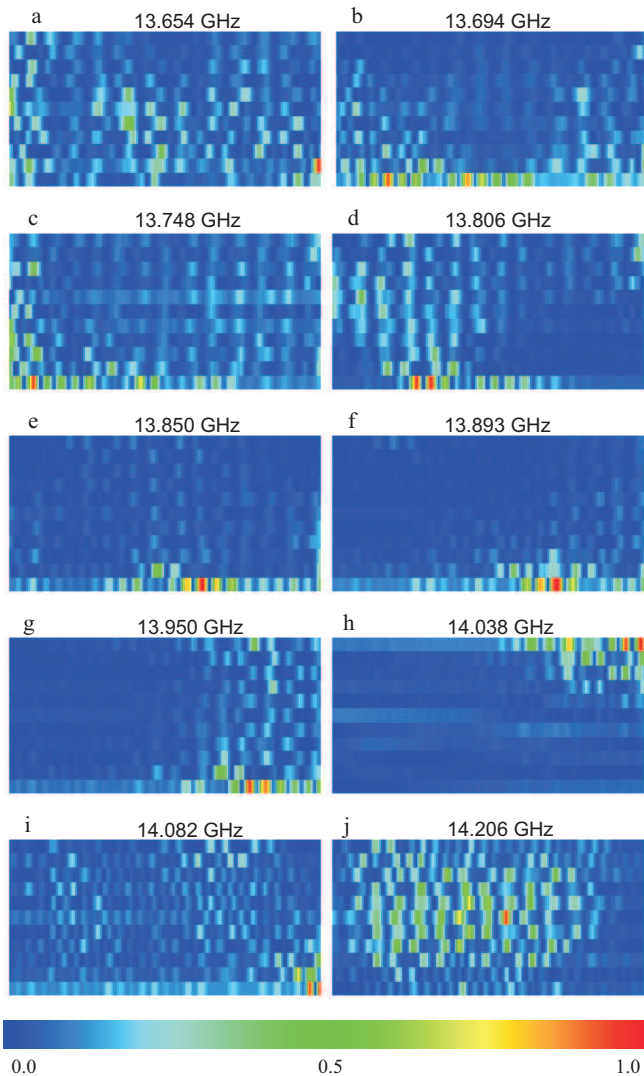


FIG. 8: (Color online) The electric field intensity distributions measured at the resonance frequencies in Fig. 7. These are marked with arrows and the labels ranging from a→j. The blue (darkest) color corresponds to the lowest, the red (brightest) to the highest intensity.

III. SUMMARY

In summary, we have observed experimentally the anomalous $1/L$ scaling behavior of the transmission of electromagnetic waves through a photonic crystal, which were excited at the Dirac frequency and sent onto the crystal in ΓK direction, that is, at a conically shaped singularity of the photonic band structure. Furthermore, for the first time we implemented an experimental setup representing a microwave analogue of a Dirac billiard, that is a relativistic quantum billiard. We have observed experimentally states localized at edges of the Dirac billiard, which correspond to the edge states occurring at zigzag edges in graphene flakes.

For the study of the spectral properties of Dirac billiards of different shapes we plan to perform measurements with superconducting Dirac billiards at liquid helium temperature. The aim is the study of the effect of the shape of a Dirac billiard and the edge structure of the enclosed photonic crystal on its spectral properties. Another interesting aspect concerning properties of the wave functions is the scarring phenomenon which has been seen numerically in graphene flakes with the shape of a stadium⁴³.

IV. ACKNOWLEDGEMENTS

The authors thank E. Bogomolny and T. Tudorovskiy for stimulating discussions, and the LPTMS in Orsay for its hospitality. This work has been supported by the DFG within the SFB 634.

* Electronic address: dietz@ikp.tu-darmstadt.de

† Electronic address: richter@ikp.tu-darmstadt.de

¹ K. S. Novoselov, A. K. Geim, S. V. Morozov, D. Jiang, Y. Zhang, S. V. Dubonos, I. V. Grigorieva, and A. A. Firsov, *Science* **306**, 666 (2004).

² P. R. Wallace, *Phys. Rev.* **71**, 622 (1947).

³ H.-P. Boehm, R. Setton, and E. Stumpp, *Pure Appl. Chem.* **66**, 1893 (1994).

⁴ A. H. Castro Neto, F. Guinea, N. M. R. Peres, K. S. Novoselov, and A. K. Geim, *Rev. Mod. Phys.* **81**, 109 (2009).

⁵ C. W. J. Beenakker, *Rev. Mod. Phys.* **80**, 1337 (2008).

⁶ J. C. Slonczewski and P. R. Weiss, *Phys. Rev.* **109**, 272 (1958).

⁷ S. Joannopoulos, J. D. Johnson, R. Meade, and J. Winn, *Photonic Crystals. Molding the Flow of Light* (Princeton University Press, Princeton and Oxford, 2008), 2nd ed.

⁸ S. Raghu and F. D. M. Haldane, *Phys. Rev. A* **78**, 033834 (2008).

⁹ E. I. Smirnova, C. Chen, M. A. Shapiro, J. R. Sirigiri, and R. J. Temkin, *J. Appl. Phys.* **91**, 960 (2002).

¹⁰ M. Katsnelson, *Mater. Today* **10**, 20 (2007).

¹¹ K. S. Novoselov, A. K. Geim, S. V. Morozov, D. Jiang, M. I. Katsnelson, I. Grigorieva, S. V. Dubonos, and A. A. Firsov, *Nature* **438**, 197 (2005).

¹² P. Gaspard and S. A. Rice, *J. Chem. Phys.* **90**, 2255 (1989).

¹³ L. Brey and H. A. Fertig, *Phys. Rev. B* **73**, 235411 (2006).

¹⁴ T. Ando, *J. Phys. Soc. Jap.* **74**, 777 (2005).

- ¹⁵ S. R. Zandbergen and M. J. A. de Dood, Phys. Rev. Lett. **104**, 043903 (2010).
- ¹⁶ U. Kuhl, S. Barkhofen, T. Tudorovskiy, H.-J. Stöckmann, T. Hossain, L. de Forges de Parny, and F. Mortessagne, Phys. Rev. B **82**, 094308 (2010).
- ¹⁷ S. Bittner, B. Dietz, M. Miski-Oglu, P. Oria Iriarte, A. Richter, and F. Schäfer, Phys. Rev. B **82**, 014301 (2010).
- ¹⁸ X. Zhang and Z. Liu, Phys. Rev. Lett. **101**, 264303 (2008).
- ¹⁹ R. A. Sepkhanov, Y. B. Bazaliy, and C. W. J. Beenakker, Phys. Rev. A **75**, 063813 (2007).
- ²⁰ J. Tworzydło, B. Trauzettel, M. Titov, A. Rycerz, and C. W. J. Beenakker, Phys. Rev. Lett. **96**, 246802 (2006).
- ²¹ M. I. Katsnelson, Eur. Phys. J. B **51**, 157 (2006).
- ²² K. Nakada, M. Fujita, G. Dresselhaus, and M. S. Dresselhaus, Phys. Rev. B **54**, 17954 (1996).
- ²³ J. Wurm, K. Richter, and I. Adagideli, Phys. Rev. B **84**, 075468 (2011).
- ²⁴ L. A. Ponomarenko, F. Schedin, M. I. Katsnelson, R. Yang, E. W. Hill, K. S. Novoselov, and A. K. Geim, Science **320**, 5874 (2008).
- ²⁵ J. Wurm, A. Rycerz, İ. Adagideli, M. Wimmer, K. Richter, and H. U. Baranger, Phys. Rev. Lett. **102**, 056806 (2009).
- ²⁶ F. Libisch, C. Stampfer, and J. Burgdörfer, Phys. Rev. B **79**, 115423 (2009).
- ²⁷ A. R. Akhmerov and C. W. J. Beenakker, Phys. Rev. B **77**, 085423 (2008).
- ²⁸ S. Sridhar, Phys. Rev. Lett. **67**, 785 (1991).
- ²⁹ A. Richter, in *Emerging Applications of Number Theory*, The IMA Volumes in Mathematics and its Applications, edited by D. A. Hejhal, J. Friedmann, M. C. Gutzwiller, and A. M. Odlyzko (Springer, New York, 1999), vol. 109, p. 479.
- ³⁰ H.-J. Stöckmann, *Quantum Chaos: An Introduction* (Cambridge University Press, Cambridge, 2000).
- ³¹ B. Dietz, T. Friedrich, M. Miski-Oglu, A. Richter, and F. Schäfer, Phys. Rev. E **75**, 035203 (2007).
- ³² B. Dietz, T. Friedrich, H. L. Harney, M. Miski-Oglu, A. Richter, F. Schäfer, and H. A. Weidenmüller, Phys. Rev. E **81**, 036205 (2010).
- ³³ U. Kuhl, H.-J. Stöckmann, and R. Weaver, J. Phys. A **38**, 10433 (2005).
- ³⁴ G. E. Mitchell, A. Richter, and H. A. Weidenmüller, Rev. Mod. Phys. **82**, 2845 (2010).
- ³⁵ L.-G. Wang, Z.-G. Wang, J.-X. Zhang, and S.-Y. Zhu, Opt. Lett. **34**, 1510 (2009).
- ³⁶ M. V. Berry and R. J. Mondragon, Proc. R. Soc. London A **412**, 53 (1987).
- ³⁷ H.-D. Gräf, H. L. Harney, H. Lengeler, C. H. Lewenkopf, C. Rangacharyulu, A. Richter, P. Schardt, and H. A. Weidenmüller, Phys. Rev. Lett. **69**, 1296 (1992).
- ³⁸ C. Dembowski, B. Dietz, T. Friedrich, H.-D. Gräf, H. L. Harney, A. Heine, M. Miski-Oglu, and A. Richter, Phys. Rev. E **71**, 046202 (2005).
- ³⁹ A. Gokirmak, D.-H. Wu, J. S. A. Bridgewater, and S. M. Anlage, Rev. Sci. Instrum. **69**, 3410 (1998).
- ⁴⁰ C. Dembowski, H.-D. Gräf, R. Hofferbert, H. Rehfeld, A. Richter, and T. Weiland, Phys. Rev. E **60**, 3942 (1999).
- ⁴¹ L. C. Maier and J. C. Slater, J. Appl. Phys. **23**, 68 (1952).
- ⁴² E. Bogomolny, B. Dietz, T. Friedrich, M. Miski-Oglu, A. Richter, F. Schäfer, and C. Schmit, Phys. Rev. Lett. **97**, 254102 (2006).
- ⁴³ L. Huang, Y.-C. Lai, D. K. Ferry, S. M. Goodnick, and R. Akis, Phys. Rev. Lett. **103**, 054101 (2009).